Characterization of regional brain metabolic changes in metastatic melanoma using ^{18}F-FDG PET/CT imaging: A case report

Om H. Gandhi[1*] MS, Jaskeerat Gujral[1*] MSE, Amir A. Amanullah[1] MD, Shiv Patil[1,2] MS, Robert C Subtirelu[1] Msc, Eric M Teichner[1,2] BA, Sedra Abou Ali Mhana[1] MD, Thomas J. Werner[1] MSE, Abass Alavi[1] MD, Mona-Elisabeth Revheim[3,4] MD, PhD, MHA

**Authors contributed equally*

1. Department of Radiology, University of Pennsylvania, Philadelphia, PA, USA
2. Sidney Kimmel Medical College, Thomas Jefferson University, Philadelphia, PA, USA
3. The Intervention Center, Rikshospitalet, Division for Technology and Innovation, Oslo University Hospital, 0424 Oslo, Norway;
4. Institute of Clinical Medicine, Faculty of Medicine, University of Oslo, 0313 Oslo, Norway

Keywords: Metastatic melanoma - Brain metastases - ^{18}F-FDG PET/CT - MIMneuro - Diaschisis - Vasogenic edema

Corresponding author:
Mona-Elisabeth Revheim, MD, PhD, MHA,
Institute of Clinical Medicine, University of Oslo, Postbox 1078, Blindern, 0316 Oslo, Norway; The Intervention Center, Rikshospitalet, Post box 4950 Nydalen, 0424 Oslo, Norway.
m.e.rootwelt-revheim@medisin.uio.no; mona.elisabeth.revheim@ous-hf.no

Received:
24 November 2025
Accepted:
13 April 2026

Abstract

Brain metastases occur in 40%-60% of melanoma patients and represent a major clinical challenge with historically poor prognosis. While conventional neuroimaging modalities such as magnetic resonance imaging (MRI) delineate metastases with high specificity, they cannot capture the widespread cerebral metabolic disruptions that underlie neurological impairment associated with infiltrative lesions. This case report demonstrates the utility of fluorine-18-fluorodeoxyglucose (^{18}F-FDG) positron emission tomography-computed tomography (PET/CT) in characterizing regional brain metabolic changes in metastatic melanoma. We present a case of a 78-year-old female diagnosed with metastatic melanoma who underwent ^{18}F-FDG PET/CT restaging. The imaging findings revealed hypometabolism in regions adjacent to hypoattenuation in the left occipital area, which was subsequently confirmed as a discrete parietal lobe metastasis on MRI. Quantitative assessment using MIMneuro software across 84 brain regions revealed diffuse metabolic disturbances extending beyond the focal lesion. The most pronounced hypometabolism was observed in the cingulate gyri (z=-4.47), cerebellum (z=-2.29), pons (z=-2.22), and temporal regions (z=-2.18). In contrast, marked hypermetabolism was noted in occipital and parietal regions (z=5.71). These widespread patterns support the concept that brain metastases can result in systemic neurological deficits, disrupting mechanisms related to diaschisis, vascular regulation, and immune-mediated pathways. These findings highlight the utility of ^{18}F-FDG PET/CT in uncovering functional brain alterations not visible on conventional imaging, offering potential value in clinical decision making and disease assessment of melanoma patients with brain metastases

Hell J Nucl Med 2026; 29(1): 34-38 *Epub ahead of print: 7 April 2026* *Published online: 30 April 2026*

Introduction

Melanoma is the third most common cause of brain metastases, with central nervous system (CNS) involvement occurring in approximately 40% to 60% of patients with melanoma [1, 2]. Among solid malignancies, melanoma has the highest propensity for CNS metastasis [3]. Although historically, clinical data has reported a median survival rate of 4 to 5 months, the recent introduction of novel checkpoint inhibitors and targeted therapies has extended the median survival to 12.8 months [4, 5]. Activating oncogenic B-raf proto-oncogene (BRAF) mutations are present in up to 50% of metastatic melanoma cases and play a key role in supporting tumor cells to survive within the brain microenvironment [6, 7] . Melanoma cells can cross the blood-brain barrier and, once within the brain, rely on vascular mimicry rather than traditional angiogenesis, with recent studies showing increased vascular mimicry density in brain metastases compared to other sites [8-10].

Conventional neuroimaging modalities provide limited information about functional consequences beyond identifying visible lesions. Magnetic resonance imaging (MRI) detects structural changes such as vasogenic edema and mass effect but has propensity to miss broader metabolic disruption throughout neural networks. This limitation is clinically relevant as patients with melanoma brain metastases often present with neurological symptoms and cognitive impairment that are excessive for their anatomical size and location, indicating widespread functional effects not visible on standard imaging [11].

Fluorine-18-fluorodeoxyglucose (^{18}F-FDG) positron emission tomography-computed tomography (PET/CT) evaluates glucose metabolism in melanoma, detecting functional disruption that may precede or extend beyond anatomical changes. While well-established for staging and treatment monitoring, important limitations include size-dependent

sensitivity (100% for metastases ≥10mm, 83% for 6-10mm, and only 23% for lesions ≤5mm) [12, 13] and false-positive findings from inflammatory processes. Despite these constraints, ^{18}F-FDG PET provides valuable clinical applications including treatment response prediction through metabolic flare (immune activation) or metabolic response (tumor cell death) within one week of starting immunotherapy [14], with residual metastases showing uptake in 56% of cases (62% confirmed melanoma, 38% treatment-related immune infiltrates) [15]. Quantitative biomarkers such as total metabolic tumor volume (MTV) offer prognostic value, with high MTV (>5.6cm^3) inversely associated with survival; when combined with radiomic parameters, MTV stratifies patients into risk categories with survival rates of 91.1%, 56.1%, and 19% for low, intermediate, and high-risk groups, respectively [16-18], providing cost-effective prognostic information to complement conventional clinical assessment.

Case presentation

We present the case of a 78-year-old woman with metastatic melanoma who underwent ^{18}F-FDG PET/CT restaging three months after baseline imaging. During this interval, she received multiple cycles of chemotherapy and remained in good health and was clinically stable, without neurologic symptoms nor focal neurologic deficits. A restaging scan was obtained to assess treatment response and evaluate disease progression.

Patient preparation followed institutional ^{18}F-FDG PET protocol. She fasted for more than 4 hours, and pre-injection glucose was confirmed to be <200mg/dL to minimize insulin-mediated glucose uptake and enhance tumor-to-background contrast. A weight-adjusted dose of 14.98mCi (554 MBq) of ^{18}F-FDG was administered intravenously. Imaging was performed 71 minutes after ^{18}F-FDG administration using a Siemens Biograph scanner, with the uptake interval selected to ensure adequate tracer interval while maintaining acceptable signal-to-noise ratios. Whole-body PET/CT was performed to assess both regional brain metabolism and systemic disease burden. The CT component provided attenuation correction and anatomical localization, with parameters optimized to achieve sufficient detail while minimizing radiation exposure. Baseline ^{18}F-FDG PET, which revealed marked hypermetabolism in area adjacent to the metastatic lesion is depicted in Figure 1.

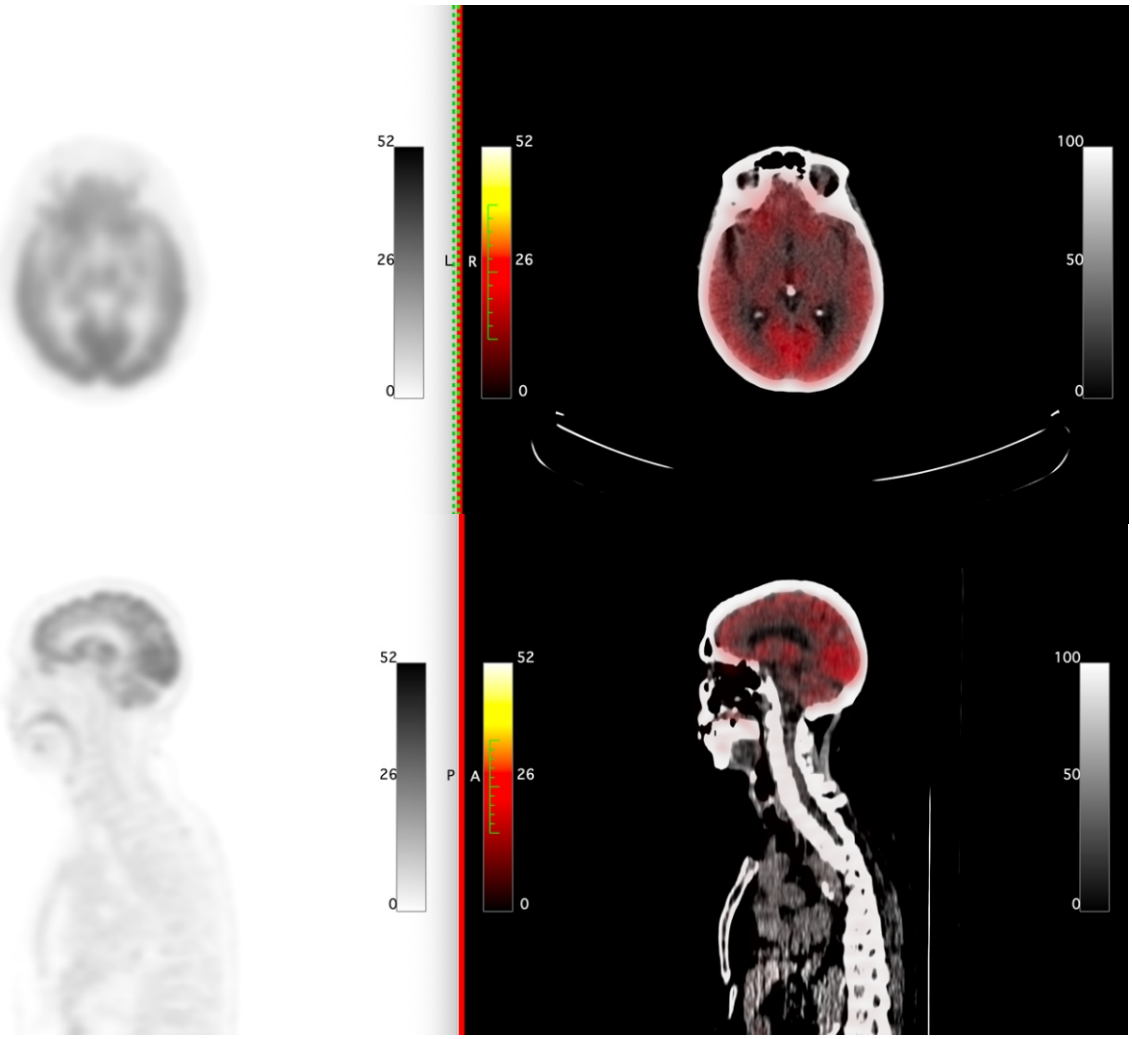

Figure 1. Baseline ^{18}F-FDG PET (Panel A,C) and fused PET/CT (Panel B,D) imaging scans reveal marked hypermetabolism in the region surrounding the metastatic lesion.

In the following month (4 months post-baseline), the patient underwent brain MRI to provide anatomical correlation, depicted in Figure 2. Pre and post contrast T1-weighted images, along with fluid-attenuated inversion recovery (FLAIR), sequences were obtained to identify brain metastases and vasogenic edema. Image acquisition was timed close to PET imaging to allow interval comparison and maintain a reasonable temporal correlation with metabolic data. Baseline CT showed no CNS metastatic disease. However, ^{18}F-FDG PET revealed hypometabolism in the region of hypoattenuation extending from the left occipital horn. This metabolic abnormality was subtle, but apparent, when compared to the contralateral hemisphere. Subsequent MRI confirmed a discrete lesion in the left parietal lobe, validating PET findings. MRI also showed vasogenic edema in the left occipital lobe white matter extending into the centrum semiovale of the left parietal lobe, depicted in Figure 3. This edema pattern indicated that metabolic changes on PET reflected broader tissue disruption beyond the tumor itself.

Analysis

Quantitative data was analyzed using MIMneuro software version 7.1.5, which provided automated, reproducible assessment of regional brain metabolism. PET images were registered to a standardized brain template to ensure precise anatomical localization and facilitate comparison with normative datasets. We analyzed 84 predefined brain regions which corresponded to established anatomical and functional territories. This comprehensive coverage included cortical areas, subcortical nuclei, and white matter regions. Standardized uptake values (SUV) were generated for each region of interest and converted to z-scores using age-matched healthy, normal controls. Brain regions adjacent to the visible metastatic lesion were excluded from analysis to minimize potential confounding effects. Z-scores were applied to standardize findings across patients and to detect subtle metabolic changes which were not evident on visual inspection. This approach converted subjective interpretation into objective quantification, enhancing both reproducibility and sensitivity.

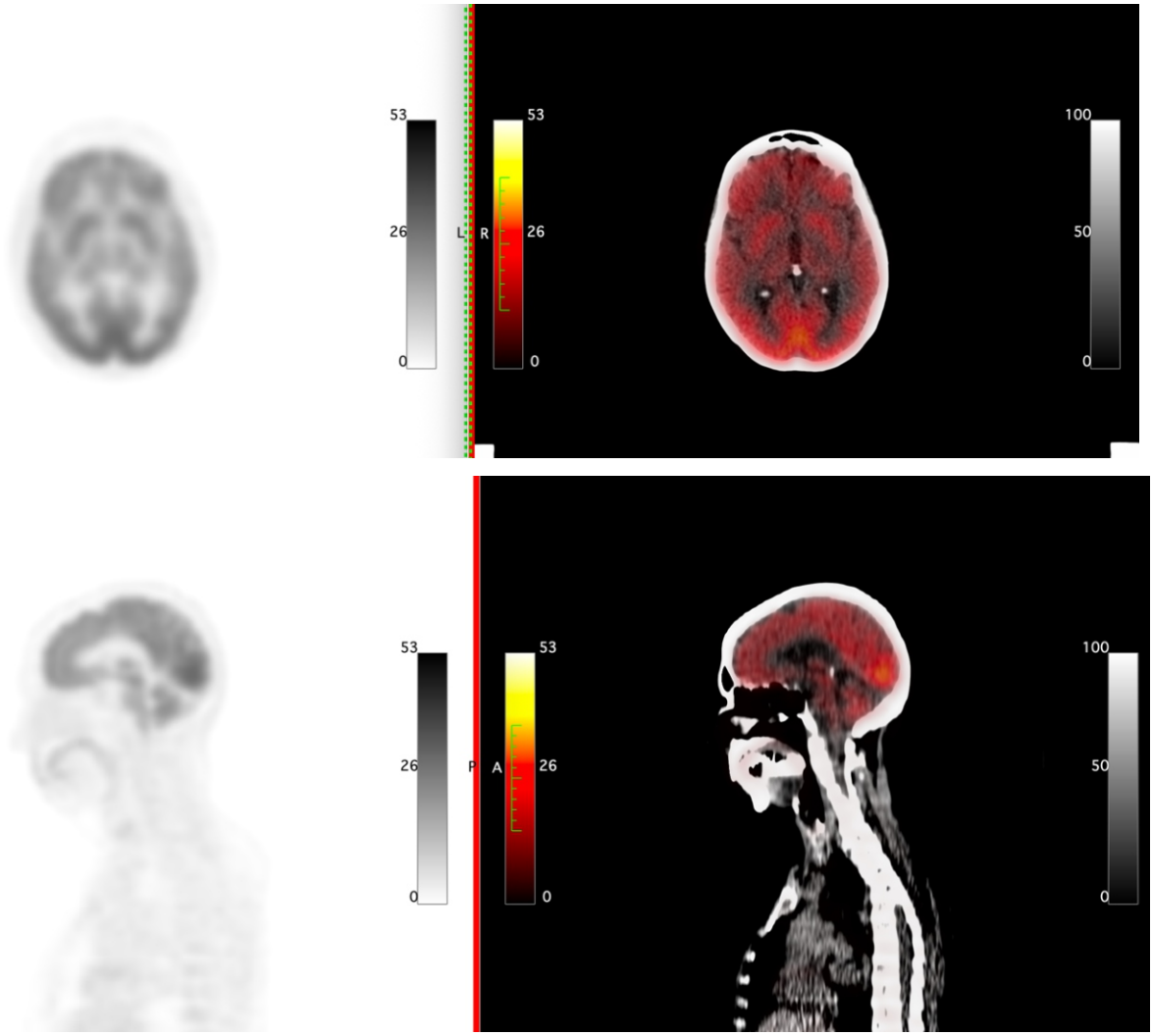

Figure 2. Restaging (Panel A,C) ^{18}F-FDG PET and (Panel B,D) PET/CT scans 4 months after baseline imaging. Reduced glucose metabolism is seen in the cingulate gyrus, cerebellum, pons, and temporal regions. In contrast, the occipitoparietal region demonstrates marked hypermetabolism bilaterally.

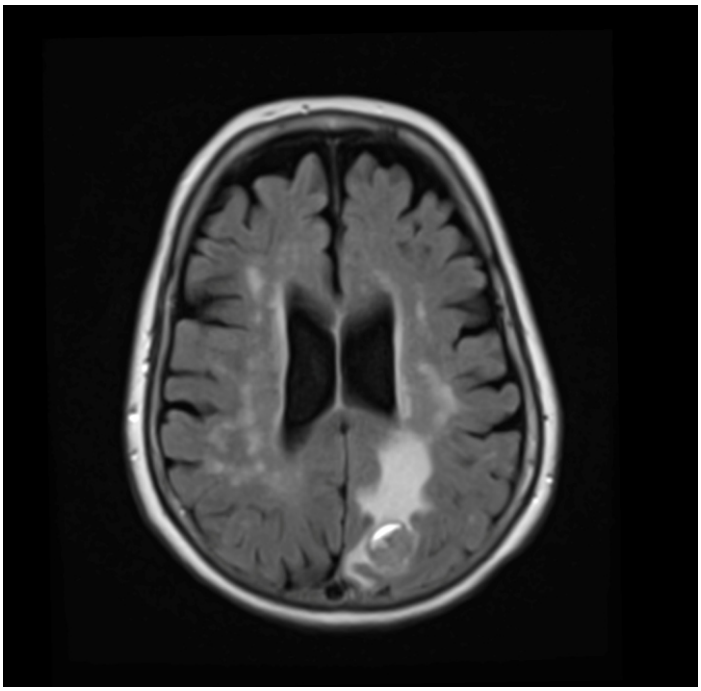

Figure 3. Depiction of FLAIR MRI sequence demonstrating a metastatic lesion in the left occipitoparietal region with surrounding vasogenic edema extending into the centrum semiovale of the left parietal lobe.

Quality control involved verifying image registration, evaluating motion artifacts, and ensuring that regions of interest accurately encompassed the intended anatomical structures. Automated outputs were reviewed by a fellowship trained attending radiologist and nuclear medicine trained attending physician to identify technical factors that could compromise quantitative accuracy.

Results and Discussion

Quantitative analysis using MIMneuro software across 84 brain regions demonstrated that metabolic alterations extended beyond the visible metastatic lesion, consistent with widespread neural network disruption. Both hypo- and hypermetabolic regions were identified, reflecting heterogeneous functional changes and suggesting coexistence of distinct pathophysiological processes. These patterns highlight brain metastases as systemic neurological conditions rather than focal lesions, with widespread alterations in regions distant from the anatomical lesion suggesting disruption of neural networks through mechanisms extending beyond direct mass effect.

The most pronounced hypometabolism occurred in the cingulate gyri (z=-4.47), a key limbic system component involved in emotional regulation, attention, and cognitive processing [19, 20]. The cerebellum (z=-2.29) and pons (z=-2.22) exhibited significant metabolic reduction, which could predispose to gait disturbances or subtle cognitive deficits given the cerebellum's role beyond motor control [21]. Temporal regions demonstrated hypometabolism (z=-2.18) in areas essential for language and memory formation. In contrast, occipital and parietal visual processing regions exhibited marked hypermetabolism (z=5.71), with the primary visual cortex demonstrating elevated activity (z=4.54).

Multiple mechanisms likely underlie the observed hypometabolism. Diaschisis, in which structurally intact regions become dysfunctional due to loss of input from connected areas, likely contributes to the metabolic suppression seen in regions distant from the tumor [22, 23]. Vasogenic edema has also been well-established as a cause of regional cortical and subcortical hypometabolism on ^{18}F-FDG PET imaging. Prior work by Powe et al. (1992) and Pourdehnad et al. (2011) demonstrated strong correlation between edema on CT/MRI and hypometabolism on ^{18}F-FDG PET, including data from a 29-patient cohort published by our group [24, 25]. In our ca-se, brain MRI showed FLAIR hyperintensity consistent with vasogenic edema in the left occipital white matter extending into the left parietal centrum semiovale, supporting that the edema in Figure 3 is associated with the observed metabolic suppression.

Several mechanisms may also underlie the hypermetabolism observed in visual processing regions. Compensatory responses to network disruption could enhance visual cortical activity to preserve function despite altered inputs. Local inflammatory responses surrounding the metastatic lesion may contribute [26], as may subclinical seizure activity originating from the tumor site [27]. Vascular alterations are another potential mechanism; notably, melanoma brain metastases exhibit greater vascular mimicry density than tumors at other sites [10], which may influence regional metabolism by modifying blood flow and nutrient delivery [28]. Additionally, the distinct immune microenvironment of brain

metastases, characterized by immune suppression and localized inflammation, likely contributes to these metabolic patterns [29].

Taken together, the ability of PET to detect these widespread functional changes underscores its potential clinical utility. Quantitative metabolic imaging can identify functional impairment earlier than conventional imaging, guide treatment monitoring, and support prognostic assessment. Anti-PD-1 antibodies achieve intracranial response rates of 20%-30% in patients with brain metastases, and early ^{18}F-FDG PET within one week of initiating immunotherapy can predict response through metabolic flare or suppression [14, 30]. Quantitative metabolic parameters can augment clinical prognostic models accounting for performance status, lesion number, and extracranial disease [31, 32]. Future research should validate these findings in larger cohorts, examine correlations with clinical outcomes, and integrate metabolic imaging with other modalities such as diffusion tensor imaging to provide comprehensive assessment of brain network disruption.

Bibliography

1. Eroglu Z, Holmen SL, Chen Q et al. Melanoma central nervous system metastases: An update to approaches, challenges, and opportunities. *Pigment Cell Melanoma Res* 2019; 32: 458-69.
2. Tan XL, Le A, Tang H et al. Burden and Risk Factors of Brain Metastases in Melanoma: A Systematic Literature Review. *Cancers (Basel)* 2022; 14: 6108.
3. Cohen JV, Tawbi H, Margolin KA et al. Melanoma central nervous system metastases: current approaches, challenges, and opportunities. *Pigment Cell Melanoma Res* 2016; 29: 627-42.
4. Vosoughi E, Lee JM, Miller JR et al. Survival and clinical outcomes of patients with melanoma brain metastasis in the era of checkpoint inhibitors and targeted therapies. *BMC Cancer* 2018; 18: 490.
5. Rieth JM, Swami U, Mott SL et al. Melanoma Brain Metastases in the Era of Targeted Therapy and Checkpoint Inhibitor Therapy. *Cancers (Basel)* 2021; 13: 1489.
6. Castellani G, Buccarelli M, Arasi MB et al. BRAF Mutations in Melanoma: Biological Aspects, Therapeutic Implications, and Circulating Biomarkers. *Cancers (Basel)* 2023; 15: 4026.
7. Caruso G, Garcia Moreira CG, Iaboni E et al. Tumor Microenvironment in Melanoma Brain Metastasis: A New Potential Target? *Int J Mol Sci* 2025; 26: 5018.
8. Abate-Daga D, Ramello MC, Smalley I et al. The biology and therapeutic management of melanoma brain metastases. *Biochem Pharmacol* 2018; 153: 35-45.
9. Fazakas C, Wilhelm I, Nagyoszi P et al. Transmigration of melanoma cells through the blood-brain barrier: role of endothelial tight junctions and melanoma-released serine proteases. *PLoS One* 2011; 6: e20758.
10. Provance OK, Oria VO, Tran TT et al. Vascular mimicry as a facilitator of melanoma brain metastasis. *Cell Mol Life Sci* 2024; 81: 188.
11. Pope WB. Brain metastases: neuroimaging. *Handb Clin Neurol* 2018; 149: 89-112.
12. Tchernev G, Popova LV. PET Scan Misses Cutaneous Melanoma Metastasis with Significant Tumour Size and Tumour Thickness. *Open Access Maced J Med Sci* 2017; 5: 963-6.
13. Filippi L, Bianconi F, Schillaci O et al. The Role and Potential of ^{18}F-FDG PET/CT in Malignant Melanoma: Prognostication, Monitoring Response to Targeted and Immunotherapy, and Radiomics. *Diagnostics (Basel)* 2022; 12: 929.
14. Anderson TM, Chang BH, Huang AC et al. ^{18}F-FDG PET/CT Imaging 1 Week after a Single Dose of Pembrolizumab Predicts Treatment Response in Patients with Advanced Melanoma. *Clin Cancer Res* 2024; 30: 1758-67.
15. Kong BY, Menzies AM, Saunders CA et al. Residual ^{18}F-FDG PET metabolic activity in metastatic melanoma patients with prolonged response to anti-PD-1 therapy. *Pigment Cell Melanoma Res* 2016; 29: 572-7.
16. Flaus A, Habouzit V, De Leiris N et al. ^{18}F-FDG PET biomarkers for prediction of survival in metastatic melanoma prior to anti-PD1 immunotherapy. *Sci Rep* 2021; 11: 18795.
17. Ito K, Schoder H, Teng R et al. Prognostic value of baseline metabolic tumor volume measured on ^{18}F-fluorodeoxyglucose positron emission tomography/computed tomography in melanoma patients treated with ipilimumab therapy. *Eur J Nucl Med Mol Imaging* 2019; 46: 930-9.
18. Annovazzi A, Ferraresi V, Rea S et al. Prognostic value of total metabolic tumour volume and therapy-response assessment by ^{18}F-FDG PET/CT in patients with metastatic melanoma treated with BRAF/MEK inhibitors. *Eur Radiol* 2022; 32: 3398-407.
19. Rolls ET. The cingulate cortex and limbic systems for emotion, action, and memory. *Brain Struct Funct* 2019; 224: 3001-18.
20. van Veen V, Cohen JD, Botvinick MM et al. Anterior cingulate cortex, conflict monitoring, and levels of processing. *Neuroimage* 2001; 14: 1302-8.
21. Zhang P, Duan L, Ou Y et al. The cerebellum and cognitive neural networks. *Front Hum Neurosci* 2023; 17: 1197459.
22. Guell X, Schmahmann JD. Diaschisis in the human brain reveals specificity of cerebrocerebellar connections. *J Comp Neurol* 2023; 531: 2185-93.
23. Carrera E, Tononi G. Diaschisis: past, present, future. *Brain* 2014; 137: 2408-22.
24. Powe JE, Alavi JB, Alavi A et al. Cerebral Metabolic Changes in Patients with Brain Tumors Demonstrated by Positron Emission Tomography. *J Neuroimaging* 1992; 2: 1-7.
25. Pourdehnad M, Basu S, Duarte P et al. Reduced grey matter metabolism due to white matter edema allows optimal assessment of brain tumors on ^{18}F-FDG PET. *Hell J Nucl Med* 2011; 14: 219-23.
26. Block F, Dihne M, Loos M. Inflammation in areas of remote changes following focal brain lesion. *Prog Neurobiol* 2005; 75: 342-65.
27. Wang J, Zhang Y, Sun H, Cui R. Hypermetabolism Caused by Seizure Mimicking Tumor Recurrence. *Clin Nucl Med* 2018; 43: 930-2.
28. Ferda J, Frolich M, Ferdova E et al. Neovascularization, vascular mimicry and molecular exchange: The imaging of tumorous tissue aggressiveness based on tissue perfusion. *Eur J Radiol* 2023; 163: 110797.
29. Fischer GM, Jalali A, Kircher DA et al. Molecular Profiling Reveals Unique Immune and Metabolic Features of Melanoma Brain Metastases. *Cancer Discov* 2019; 9: 628-45.
30. Kamath SD, Kumthekar PU. Immune Checkpoint Inhibitors for the Treatment of Central Nervous System (CNS) Metastatic Disease. *Front Oncol* 2018; 8: 414.
31. Hasanov M, Milton DR, Davies AB et al. Changes in outcomes and factors associated with survival in melanoma patients with brain metastases. *Neuro Oncol* 2023; 25: 1310-20.
32. Gumusay O, Coskun U, Akman T et al. Predictive factors for the development of brain metastases in patients with malignant melanoma: a study by the Anatolian society of medical oncology. *J Cancer Res Clin Oncol* 2014; 140: 151-7.